CrossMark

Synthesis and in vitro evaluation of an antiangiogenic cancer-specific dual-targeting ^{177}Lu-Au-nanoradiopharmaceutical

Abraham González-Ruíz[1,2] · Guillermina Ferro-Flores[1] · Erika Azorín-Vega[1] ·
Blanca Ocampo-García[1] · Flor de Maria Ramírez[1] · Clara Santos-Cuevas[1] ·
Luis De León-Rodríguez[3] · Keila Isaac-Olivé[2] · Myrna Luna-Gutiérrez[1] ·
Enrique Morales-Ávila[2]

Abstract The aim of this research was to synthesize and chemically characterize a cancer-specific ^{177}Lu-Au-nanoradiopharmaceutical based on gold nanoparticles (NPs), the nuclear localization sequence (NLS)-Arg-Gly-Asp peptide and an aptamer (HS-pentyl-pegaptanib) to target both the α(v)β(3) integrin and the vascular endothelial growth factor (VEGF) overexpressed in the tumor neovasculature, as well as to evaluate by the tube formation assay, the nanosystem capability to inhibit angiogenesis. ^{177}Lu-NP-RGD-NLS-Aptamer was obtained with a radiochemical purity of 99 ± 1%. Complete inhibition of tube formation (angiogenesis) was demonstrated when endothelial cells (EA.hy926), cultured in a 3D-extracellular matrix support, were treated with the developed nanosystem.

Keywords Lutetium-177 · ^{177}Lu-gold nanoparticles · Antiangiogenic agent · RGD · HS-pentyl-pegaptanib · VEGF inhibition · α(v)β(3) integrin

✉ Guillermina Ferro-Flores
ferro_flores@yahoo.com.mx;
guillermina.ferro@inin.gob.mx

1 Instituto Nacional de Investigaciones Nucleares, Carretera México-Toluca S/N, 52750 Ocoyoacac, Estado de México, Mexico

2 Universidad Autónoma del Estado de México, Paseo Tollocan S/N, 50180 Toluca, Estado de México, Mexico

3 The University of Auckland, 23 Symonds St, Auckland, New Zealand

Introduction

^{177}Lu-nanoradiopharmaceuticals based on gold nanoparticles (NPs) are in the spotlight of theranostic innovation. Due to their optical properties, nontoxic nature, relatively simple preparation and functionalization, NPs have been successfully labeled with ^{177}Lu (therapeutic β^-_{max} emission of 0.497 MeV and γ radiation of 0.208 MeV for diagnostic imaging) and covalently bound to molecules with target-specific recognition to obtain nanosystems with properties suitable for optical and nuclear imaging, plasmonic-photothermal therapy and targeted radiotherapy on a single platform [1–3].

Solid tumors require the formation of new blood vessels (angiogenesis) for growth, and many new cancer therapies are directed against the tumor vasculature [4, 5]. Multiple angiogenesis inhibitors have been therapeutically validated in preclinical and clinical trials [6].

The α(v)β(3) integrin is a specific marker of the neovasculature, which is overexpressed in the tumor vessels during angiogenesis. The Arg-Gly-Asp (RGD) peptide motifs have been identified as high-affinity α(v)β(3) selective ligands and therefore as antiangiogenic agents [7]. Furthermore, RGD conjugated to radiolabeled peptides with a nuclear localization peptide sequence (NLS) promote the radionuclide internalization in cancer cells overexpressing α(v)β(3) integrins, increasing the effectiveness of targeted radiotherapy [8, 9].

Aptamers are single-stranded deoxyribonucleic acid or ribonucleic acid oligonucleotides, which can bind their target with high selectivity and affinity [10]. Pegaptanib is an aptamer that inhibits angiogenesis by targeting the vascular endothelial growth factor (VEGF) pathway [11].

🍦 Springer

One of the most widely used in vitro assays to model the reorganization stage of angiogenesis is the tube formation assay. This assay measures the ability of endothelial cells to form capillary structures (tubes). The study focuses on how specific signaling molecules are involved in the three-dimensional formation of vascular networks. Compounds which inhibit the formation of tubes could be useful as specific antiangiogenic agents [12].

The use of heterobivalent molecules interacting concomitantly with different receptors in tumor cells is an approach for drug enhancement for specific and sensitive tumor imaging [13–15].

The aim of this study was to synthesize and chemically characterize a cancer-specific ^{177}Lu-Au-nanoradiopharmaceutical based on NPs, NLS-RGD and aptamer able to target both the α(v)β(3) integrin and the VEGF, as well as evaluate by the tube formation assay, the nanosystem capability to inhibit angiogenesis.

Experimental

Synthesis of the NLS-RGD peptide

The synthesis procedure is described in detail in the Supplementary information section. Briefly, the cyclo(Arg-Gly-Asp-DTyr-Lys)-3-maleimidepropionylamide (c(RGDyK)-3MP) and NH_2-Gly^1-Arg^2-Lys^3-Lys^4-Arg^5-Arg^6-Gly^7-Gly^8-Cys^9-Gly^{10}-Cys^{11}(Acm)-Gly^{12}-Cys^{13}(Acm)-CONH$_2$ (NLS-CGCGC) peptides were first synthesized and bound through the -3MP and Cys^9 to produce the NH_2-Gly-Arg-Lys-Lys-Arg-Arg-Gly-Gly-Cys-[c(Arg-Gly-Asp-D-Tyr-Lys)-3-succinimidepropionylamide)]-Gly-Cys(Acm)-Gly-Cys(Acm)-CONH$_2$ (NLS-RGD) peptide; m/z (MALDI+) m/z = 2248.18 [M + H]$^+$ (calcld. 2250.46).

Synthesis of the aptamer-SH (pegaptanib derivative)

The aptamer analogue to pegaptanib was designed to interact covalently with gold atoms on the nanoparticle surface by adding a HS-pentyl (-SH terminal group) and it was synthesized with support of the Iba Solutions Company (Germany). The sequence of the RNA aptamer is as follows: [(2′-deoxy-2′-fluoro)C-Gm-Gm-A-A-(2′-deoxy-2′-fluoro)U-(2′-deoxy-2′-fluoro)C-Am-Gm-(2′-deoxy-2′-fluoro)U-Gm-Am-Am-(2′-deoxy-2′-fluoro)U-Gm-(2′-deoxy-2′-fluoro)C-(2′-deoxy-2′fluoro)U-(2′-deoxy-2′fluoro)U-Am-(2′-deoxy-2′-fluoro)U-Am-(2′-deoxy-2′-fluoro)C-Am-(2′-deoxy-2′-fluoro)U-(2′deoxy-2′-fluoro)C-(2′-deoxy-2′-fluoro)C-Gm-(3′ → 3′)-dT], [[5-(phosphoonoxy)pentyl]thiol]. The methodology of the synthesis included: (1) standard linkage of 28 RNA bases; (2) the attachment of 2′-fluoro to every U and C, (3) the attachment of 2′-O-Methyl at 2,3,8,9,11–13,15,19,21,23 and 27; (4) inverse modification dT, (5) 5′-thiol; and (6) HPLC purification of the RNA. PM = 9197.25 g/mol. The final product was lyophilized on a scale of 29 nmol.

Conjugation of NLS-RGD and aptamer to the NPs

A NP solution stabilized with PBS (1 mL, 20 nm, 6.54×10^{11} particles/mL, Sigma Aldrich) was added to 10 μL of a NLS-RGD solution (1 mg/10 mL; 2.68×10^{14} molecules; 16 molecules per 20 nm nanoparticle) followed by 10 μL of an aptamer solution (29 nmol/10 mL; 1.767×10^{13} molecules; 27 molecules per 20 nm nanoparticle). The conjugation of the aptamer and NLS-RGD molecules to the NP was performed by reactions of the –SH with NP surface. Since up to 1701 peptides or molecules can be attached to one NP (20 nm, surface area = 1260 nm^2) [16], no further purification was necessary.

Preparation of the ^{177}Lu-Au-nanoradiopharmaceutical (^{177}Lu-NP-RGD-NLS-Aptamer)

The 1,4,7,10-tetraazacyclododecane-N,N′,N″,N‴-tetraacetic acid-Gly-Gly-Cys (DOTA-GGC) peptide to be used as chelator for Lu-177 (DOTA), was synthesized according to the method described by Luna-Gutiérrez et al. [17]. The detail methods to prepare ^{177}Lu-DOTA-GGC-NP and to evaluate its radiochemical purity have been shown elsewhere [17, 19]. To 1 mL of the NP-NLS-RGD-Aptamer solution, 3 μL (18–20 MBq) of ^{177}Lu-DOTA-GGC was added (0.25 μg of peptide; 1.89×10^{14} molecules; 270 molecules per 20 nm NP) to form the ^{177}Lu-DOTA-GGC-NP-NLS-RGD-Aptamer nanosystem (^{177}Lu-NP-NLS-RGD-Aptamer) (Fig. 1). For chemical characterization and comparative purposes, the radioactive and non-radioactive systems of DOTA-GGC-NP, DOTA-GGC-NP-NLS-RGD, DOTA-GGC-NP-Aptamer and DOTA-GGC-NP-NLS-RGD-Aptamer were also prepared using the same procedure.

Chemical characterization

The DOTA-GGC-NP-NLS-RGD-Aptamer was characterized in size and shape by transmission electron microscopy (JEOL JEM2010 HT microscope operated at 200 kV). The hydrodynamic diameter and Zeta potential were obtained by dynamic light scattering (DLS) (Nanotrac Wave, Model MN401, Microtract, FL, USA). The IR spectra were acquired on a PerkinElmer System 2000 spectrometer with an ATR platform (Pike Technologies ATR-FTIR) from 4400 to 570 cm^{-1} and 700 to 30 cm^{-1}. The nanoconjugate was measured by UV–Vis spectroscopy, monitoring the shift in the surface plasmon band with a Perkin-Elmer

Fig. 1 Overall scheme of the ^{177}Lu-NP-NLS-RGD-Aptamer nanoradiopharmaceutical
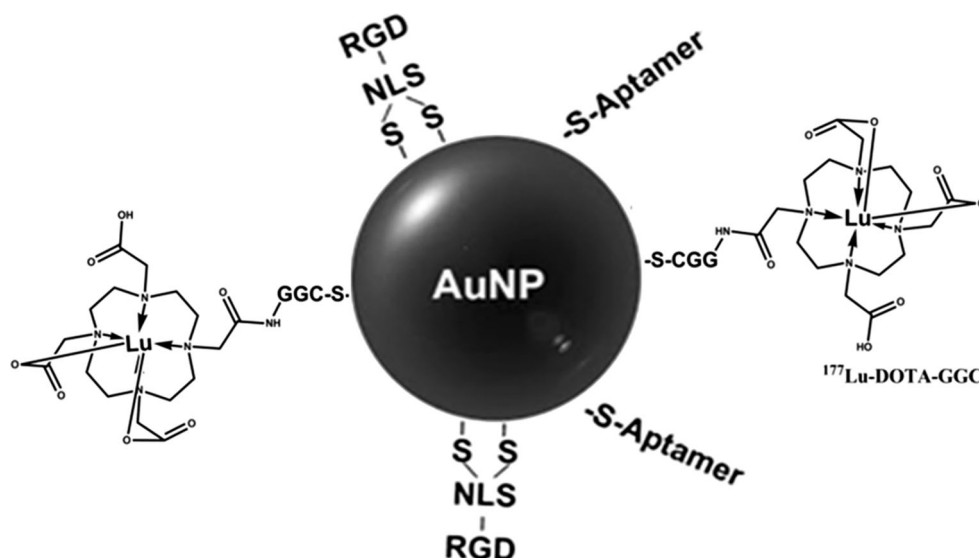
Lambda-Bio spectrometer. Raman spectra were acquired on a MicroRaman (JOBIN–Yvon-Horiba, LABRAM-HR800) spectrometer with optical microscope (OLYMPUS BX 41) and He–Ne Laser (632.8 nm) as excitation source.

Detail methods to evaluate the radiochemical purity by size-exclusion chromatography and ultrafiltration have been shown elsewhere [17, 19].

Biochemical characterization

Cell cultures

The permanent human umbilical vein cell line (EA.hy926) was purchased from Gibco-Life Technologies (Carlsbad, CA, USA) and cultured (37 °C, 5% CO_2) in F12 medium 200 (Gibco-Life Technologies). The C6 rat glioma cell line were obtained from American Type Culture Collection (Atlanta, GA, USA) and cultured (37 °C, 5% CO_2) in Roswell Park Memorial Institute Medium (Sigma-Aldrich Co.). In both cases fetal bovine serum (10%), penicillin (100 U/mL) and streptomycin (100 μg/mL) were used.

Human serum stability

Radiolabeled NP (^{177}Lu-NP-NLS-RGD-Aptamer, 200 μL) were diluted in fresh human serum and incubated at 37 °C. The stability was determined by UV–Vis analysis to monitor the NP surface plasmon at 60 min and 24 h after dilution. Radiochemical stability was determined by taking samples at 60 min and 24 h for ultrafiltration and size-exclusion evaluation (PD-10 column) as reported elsewhere [17, 19].

In vitro affinity

The method to evaluate the ^{177}Lu-NP-NLS-RGD-Aptamer affinity to α(v)β(3) integrins was carried out using the by a solid-phase binding assay as previously reported [17]. The IC_{50} value of the ^{177}Lu-NP-NLS-RGD-Aptamer peptide was determined by nonlinear regression analysis ($n = 5$) [17].

In vitro angiogenesis assay

An endothelial cell tube formation assay was performed using the ECMatrixTM kit (BD Biosciences, Bedford, MA, USA). Briefly, EA.hy926 cells (10,000 cells) were seeded onto polymerized ECMatrix and incubated at 37 °C, 5% CO_2. Cells were cultured with (CTL+) or without (CTL−) endothelial growth factor (ECGF, Sigma, Aldrich, USA, 20 μg/mL) in fetal bovine serum (FBS) and treated with DOTA-GGC-NP (10 μL, 1×10^9 nanoparticles), DOTA-GGC-NP-NLS-RGD (10 μL, 1×10^7 nanoparticles), DOTA-GGC-NP-Aptamer (10 μL, 1×10^7 nanoparticles) and DOTA-GGC-NP-NLS-RGD-Aptamer (10 μL, 1×10^7 nanoparticles). After 18 h, tube formation was analyzed under an inverted light microscope (Eclipse TE300; Nikon, Tokyo, Japan) at 40× magnification. The semi-quantitative measurement of the angiogenic potential was calculated by direct visual analysis of at least six microscopic fields for each experimental condition allowed the assignation of a numerical value to angiogenic potential that reflects the degree of remodeling by using the formula proposed by Aranda and Owen [18]. This also allowed the establishment of statistical differences in angiogenic potential between two conditions or compounds.

Internalization assay

C6 cells (1×10^6 cells/tube) were incubated (0.5 mL) with 1 kBq (1×10^7 nanoparticles) of the following treatments: (a) ^{177}Lu-NP, (b) ^{177}Lu-NP-NLS-RGD, (c) ^{177}Lu-NP-Aptamer and (d) ^{177}Lu-NP-NLS-RGD-Aptamer, in triplicate at 37 °C for 2 h. The detailed method has been shown elsewhere [16, 17]. Differences between the in vitro cell data of ^{177}Lu-NP-NLS-RGD-Aptamer and each treatment were evaluated with Student's *t* test (grouped analysis, significance was defined as $p < 0.05$).

Fluorescence microscopy images

C6 cells (0.2 mL) were incubated with the followings treatments (5×10^4 cells): (a) ^{177}Lu-NP (b) ^{177}Lu-NP-NLS-RGD, (c) ^{177}Lu-NP-Aptamer and (d) ^{177}Lu-NP-NLS-RGD-Aptamer and. In all cases 1 kBq with 1×10^7 nanoparticles was used. The detailed procedures of staining of the nuclei with Hoechst dye (blue) and the acquisition of images of fluorescent NPs internalized in the C6 cells have been shown elsewhere [21].

Results and discussion

TEM images, hydrodynamic particle size and Z potential

Images of DOTA-GGC-NP-NLS-RGD-Aptamer (NP-nanosytem) are shown in Fig. 2. The a "halo" around the NPs was observed as consequence of the poor interaction of the electron beam with the NLS-RGD and aptamer molecules (low electron density). The average particle hydrodynamic diameter of the NP-nanosystem determined by DLS was 29.99 ± 1.90 nm, which was higher than that of NP (24.70 ± 0.07 nm). The increase in the diameter also indicated the conjugation of the aptamer and NLS-RGD to the NP surface (Fig. 2) [19]. The Z potential for the NP and NP-nanosystem was -59 ± 2.7 mV and -74 ± 4.8 mV respectively, showing an increase in the colloidal stability.

Infrared and Raman spectroscopy

The MIR spectrum of the NP-nanosystem is given in Fig. 3. The spectrum is highly structured with fine bands not observed in the spectra of aptamer, NLS-RGD, DOTA-GGC nor the gold nanoparticles prior to their interaction (Fig. 3). Of interest are the multiple bands observed in the NP-nanosystem spectrum in the region from 2350 to 1700 cm^{-1} assigned to –CH$_2$NH$_3^+$, R2-NH$_2^+$, R3-NH$^+$, R–C=NH$^+$, protonated amidines (R2-N–C=N(-N)-R2)
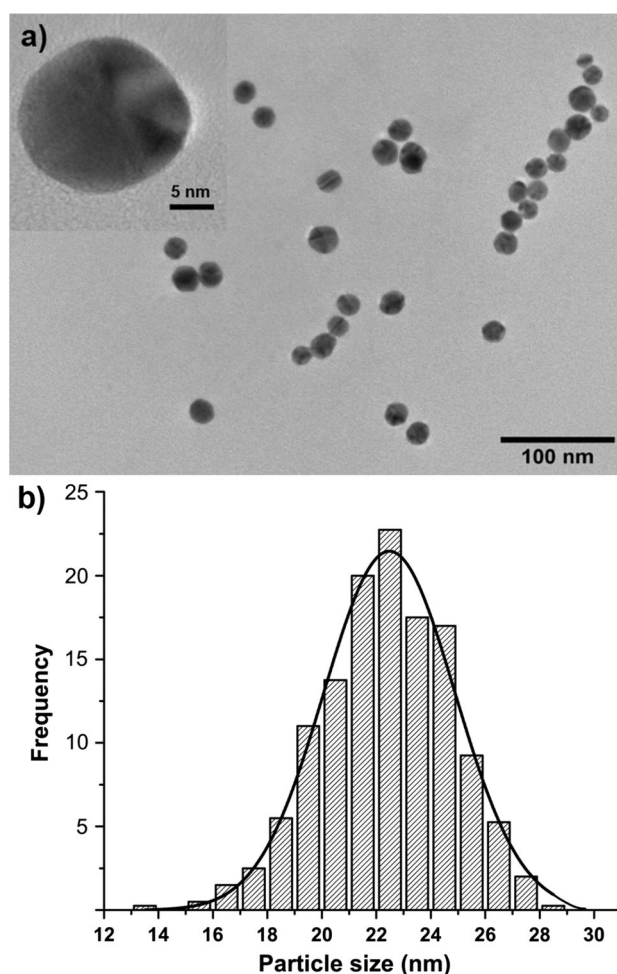

Fig. 2 **a** Transmission electron microscopy (TEM) images and **b** size distribution determined by dynamic light scattering (DLS) of the DOTA-GGC-NP-NLS-RGD-Aptamer nanosystem

from the arginine, guanine and adenine, as well as vibrations in the regions of amides I, II and III, [20]. The bands up to 3500 cm^{-1} are assigned to the unassociated –OH from the tyrosine and asparagine of the NLS-RGD and the carboxylic acid from DOTA-GGC (Fig. 3). The asymmetric vibrations (1234 cm^{-1}) in the phosphates –O–P(O)–O– bridged to the terminal pentyl mercaptan [(CH$_2$)$_5$-SH] and to the riboside (both through –CH$_2$–) observed in the aptamer spectrum disappear in the NP-nanosystem spectrum, which indicate that the aptamer is bonded to NP through the HS-pentyl moiety. In Raman spectra, the bands with good intensity confirmed the assignations in MIR. A detail analysis of the Raman, MIR and FIR spectra as evidence of the NP functionalization with the aptamer and the NLS-RGD peptide are included in the Supplementary information section.
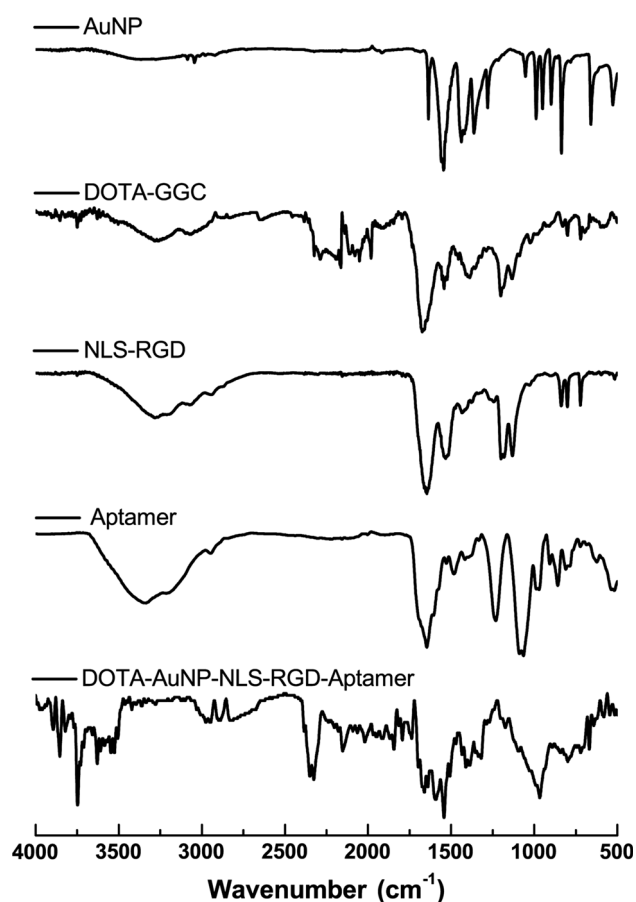
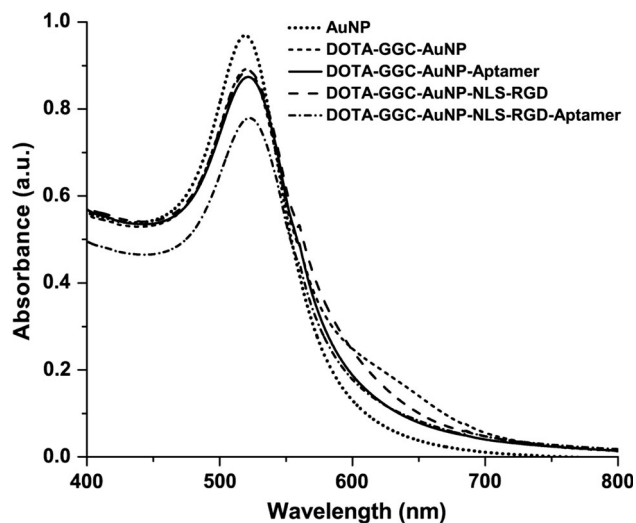**Fig. 3** MIR-Infrared spectra of NP, DOTA-GGC, NLS-RGD, Aptamer and DOTA-GGC-NP-NLS-RGD-Aptamer nanosystems

UV–Vis spectroscopy

The NP spectrum showed a characteristic surface plasmon resonance at 519.2 nm. A red-shift to 519.5, 519.8, 521.3 and 522.3 nm was observed in the DOTA-NP, DOTA-GGC-NP-Aptamer, DOTA-GGC-NP-NLS-RGD, DOTA-GGC-NP-NLS-RGD-Aptamer spectra, respectively (Fig. 4). A decrease can be noticed in the intensity of the surface plasmon resonance peak of the NP conjugates due to changes in the refraction index and dielectric medium because of the interaction between the GGC, NLS-RGD and the NP surface [21].

Radiochemical purity

Radiochemical purity of the ^{177}Lu-NP-NLS-RGD-Aptamer nanoradiopharmaceutical determined by ultracentrifugation and PD10 size-exclusion chromatography was $99 \pm 1\%$.

Human serum stability

^{177}Lu-NP-NLS-RGD-Aptamer was stable in human serum for 24 h, since at this time the radiochemical purity continues as high as $99 \pm 1\%$. The 522.3 nm surface plasmon resonance characteristic of NP, remained stable but slightly shifted to shorter energy (521.9 nm) as consequence of the protein interactions [16].

Fig. 4 UV–Vis spectra of the NP, DOTA-GGC-NP, DOTA-GGC-NP-NLS-RGD and DOTA-GGC-NP-NLS-RGD-Aptamer nanosystems
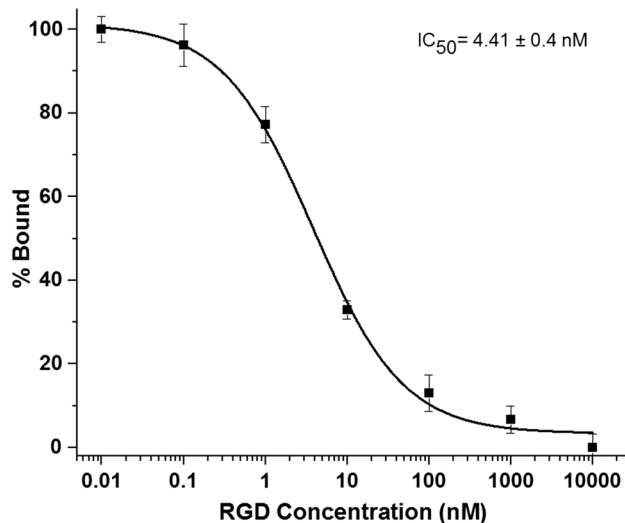
Solid-phase α(v)β(3) binding assay: in vitro affinity

Fig. 5 Competition assay of ^{177}Lu-NP-NLS-RGD-Aptamer for specific binding to the α(v)β(3) integrin

The in vitro competitive binding assay of the colloidal system ^{177}Lu-NP-NLS-RGD-Aptamer to determine the $\alpha(v)\beta(3)$ affinity showed that the concentration of the RGD peptide to displace 50% of the ^{177}Lu-NP-NLS-RGD-Aptamer from the receptor was 4.41 ± 0.4 nM (IC$_{50}$) (Fig. 5). The ^{177}Lu-NP-NLS-RGD-Aptamer affinity is congruent with similar affinity results reported for colloidal systems based on NP-RGD and radiolabeled with ^{177}Lu [17].

Endothelial cell tube formation assay

As shown in Fig. 6, cells cultured in Matrigel with proangiogenic factors (FBS and ECGF) efficiently induced flattening and cell migration (positive control, Fig. 6a), where cells reorganized and formed tubes and complex-multicellular polygonal structures, which are from two to three cells thick. Cells over Matrigel without any proangiogenic factors (negative control, Fig. 6d) remained adhered to the matrix and maintained a rounded shape.

Each of the nanosystem components [DOTA-GGC-NP (Fig. 6b); DOTA-GGC-NPs-NLS-RGD (Fig. 6c); or DOTA-GGC-NP-Aptamer (Fig. 6e)] regulated in a negative manner and with different intensity the key steps of the angiogenic process (adhesion, protrusion, cell–cell contact or cell migration). EA.hy926 cells cultured over Matrigel and stimulated with FBS and ECGF were quickly adhered and formed projections increasing cell–cell contact to migrate until forming polygonal structures that gain complexity over time (Fig. 6a).

The treatment with DOTA-GGC-NP precludes migration and reorganization of the cells, stopping the tube formation progress (Fig. 6b); furthermore, cells appear in close proximity and firmly adhere to the matrix, but polygonal structures were not formed. It has been reported that gold nanoparticles have antiangiogenic properties because they selectively interact with cell mitogens and mediators of angiogenesis, particularly blocking the VEGF165/VEGFR2 interaction [22]. The observed cell adhesion is likely to be triggered and maintained by the signaling transduction mediated by cell adhesion molecules such as integrins and its transactivation via the other growth factors present in the FBS such as EGF, which is not affected by NPs.

Exposure of cells to gold nanoparticles conjugated with the NLS-RGD peptide significantly reduced cell adhesion properties and abolished the ability of endothelial cells to form tubes even in the presence of proangiogenic stimulation (Fig. 6c). Cells exposed to DOTA-GGC-NP-NLS-RGD acquired a rounded shape, and some of them made contact, forming groups of maximum four cells (Fig. 6c). This response is certainly due to the known blocking that RGD exerts on $\alpha(v)\beta(3)$ integrin [7]. It is well known that this integrin plays key roles in cell–cell and cell–ECM interaction, this explains the lack of cell adhesion and the reduced intercellular contact. Some authors have validated
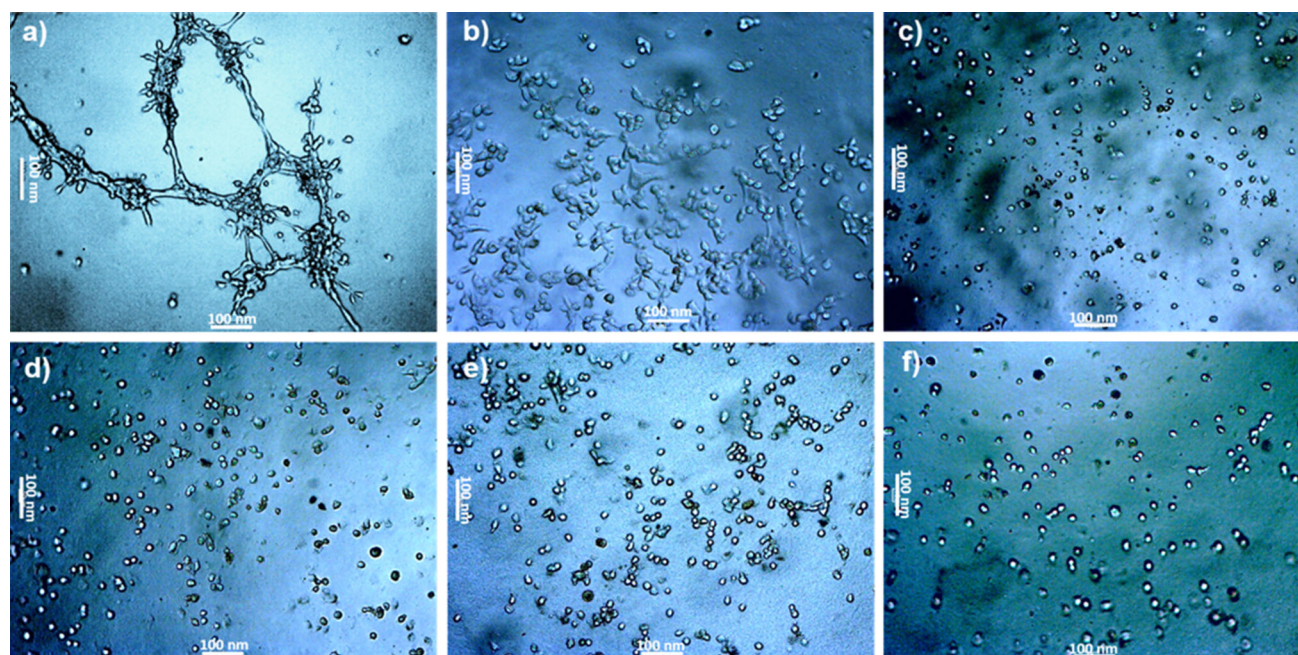

Fig. 6 Endothelial cell tube formation assay **a** without any additional treatment (positive control), and treated with **b** DOTA-GGC-NP, **c** DOTA-GGC-NP-NLS-RGD, **e** DOTA-GGC-NP-Aptamer or **f** DOTA-GGC-NP-NLS-RGD-Aptamer; **d** without proangiogenic factors (negative control)

that organelle-specific damage can be amplified by targeting molecules to the nucleus, and Kang et al. [23] have demonstrated that the DNA damage, cell division arrest and apoptosis produced by NPs could be increased by modifying NPs with the NLS sequence.

The conjugation to DOTA-GGC-NP of the RNA aptamer directed against VEGF slightly increased the antiangiogenic effect produced by the nanoparticles (Fig. 6e). Cells treated with DOTA-GGC-NP-Aptamer remained firmly attached to the matrix and approximately one-third of the population sprouted and maintained their ability to associate and form branched clusters without achieving complete formation of polygonal structures (Fig. 6e). The maintenance of cell adhesion and chemotaxis properties are due to the angiogenic signaling mediated by other growth factors, cytokines, chemokines and hormones present in the FBS.

The DOTA-GGC-NP-NLS-RGD-Aptamer nanosystem here reported, inhibits tube formation (Fig. 6f). In these culture conditions, the loss of cell adhesion, migration and protrusion was observed and very few cells could maintain contact with others.

Semi-quantitative measurement of the angiogenic potential (AP) of the tested compounds, in terms of their kinetics to bring about EA.hy926 cell line remodeling into tube structures, evidenced that a greater AP was reached by the DOTA-GGC-NP-NLS-RGD-Aptamer nanosystem with a score of 0.33 ± 0.05, which is significantly lower than that of the 2.04 ± 0.19 score obtained for the positive control, in which the maximum reorganization was observed, obtaining the formation of a complex mesh. DOTA-GGC-NP and DOTA-GGC-NP-Aptamer reduced the AP score to 0.99 ± 0.10 and 0.78 ± 0.06, respectively, while in DOTA-GGC-NP-NLS-RGD, the AP was 0.54 ± 0.08. In this study, the synergic antiangiogenic properties of a nanosystem able to simultaneously target VEGF and integrins with a remarkable ability to inhibit signals through VEGFR and interfering with its transactivation via integrins, was demonstrated.

Internalization assay

As shown in Table 1, the molecules ^{177}Lu-NP-NLS-RGD, ^{177}Lu-NP-Aptamer and ^{177}Lu-NP-NLS-RGD-Aptamer

have greater uptake and internalization than that of the unspecific molecule ^{177}Lu-NP ($p < 0.05$). Furthermore, the colloidal ^{177}Lu-NP-NLS-RGD-Aptamer system shows the largest uptake and internalization. The ^{177}Lu-NP non-specific accumulation in C6 glioblastoma cells is related to the NP passive uptake mechanism [24]. However, with the conjugation to NPs of NLS-RGD and aptamer, the specific tumor cell internalization was significantly higher (Table 1). ^{177}Lu-NP-NLS-RGD-Aptamer internalized in cell nuclei also demonstrated a specific nuclear entry (Fig. 7).

Since the C6 cell line overexpress α(v)β(3) integrin, the uptake and internalization of NLS-RGD molecules was that expected. This is in agreement with previous works in which the affinity of RGD to the α(v)β(3) integrin and NLS internalization properties have been reported [8].

At the first glance, it is difficult to understand the aptamer uptake and internalization effect, because the aptamer molecule is negatively-charged and typically, the cell membrane has negative charge characteristics. Different endocytic pathways taken by aptamer-NPs have been reported [25]. Aptamer-NPs colloidal systems, however, exhibit good cell uptake properties. Furthermore, the cell uptake and internalization of NP-aptamer has been reported to be higher than that of NPs [26]. The internalization mechanisms and intracellular trafficking of nanoparticles require further studies, especially regarding the difference between targeted and non-targeted nanoparticles.

Fluorescence microscopy images

As shown in Fig. 7, ^{177}Lu-NP-NLS-RGD-Aptamer emits the highest fluorescence, which indicates a higher NP internalization in C6 cells due to the NLS-RGD and aptamer interactions with the membrane cell. This agrees with the result of the uptake and internalization described above (Table 1). Hoechst dye inside the nuclei was visualized with an excitation filter of 330–385 nm and an emission filter of 420 nm, and the NPs were detected by using an excitation filter of 530–550 nm and an emission filter of 590 nm.

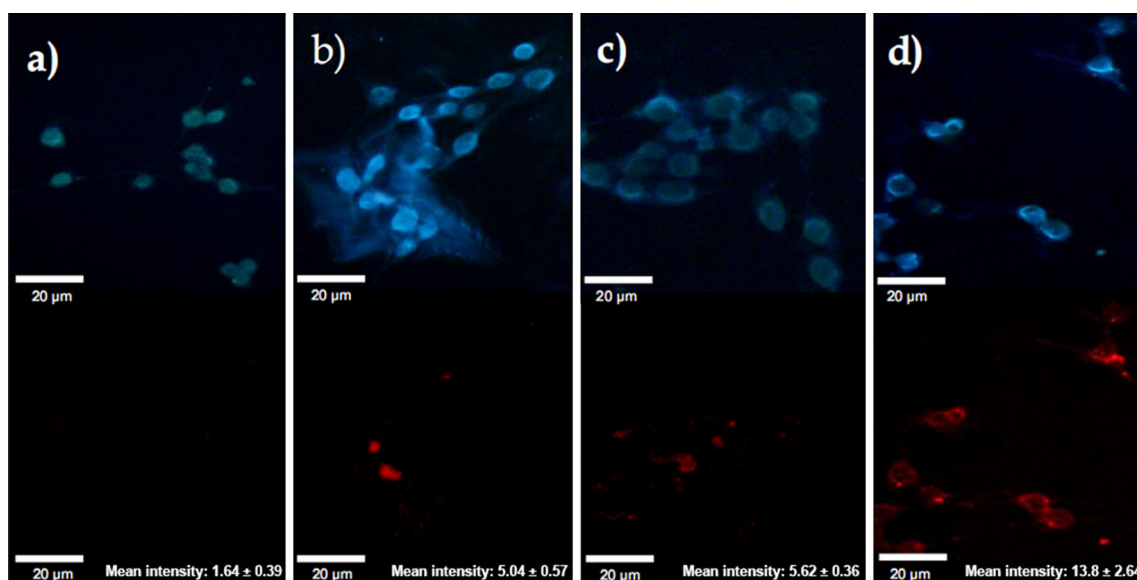The fluorescence present in the colloidal systems ^{177}Lu-NP-NLS-RGD, ^{177}Lu-NP-Aptamer and ^{177}Lu-NLS-

Table 1 Percentage of uptake and internalization of the different ^{177}Lu-nanosystems in C6 glioma cells

Treatment	Uptake (%)	Internalization (%)
^{177}Lu-NP	8.13 ± 0.72	4.04 ± 0.74
^{177}Lu-NP-NLS-RGD	15.18 ± 0.28	8.57 ± 0.26
^{177}Lu-Aptamer	14.72 ± 0.47	10.43 ± 0.06
^{177}Lu-NP-NLS-RGD-Aptamer*	20.64 ± 0.18*	17.31 ± 0.96*

* Significant statistical difference ($p < 0.05$) between ^{177}Lu-NP-NLS-RGD-Aptamer and each treatment

Fig. 7 Fluorescent images of **a** ^{177}Lu-NP, **b** ^{177}Lu-NP-NLS-RGD, **c** ^{177}Lu-NP-Aptamer and **d** ^{177}Lu-NP-NLS-RGD-Aptamer internalized in C6 cells. Observe the Hoechst dye (*blue*) inside the nuclei of cells (excitation filter of 330–385 nm, emission filter of 420 nm) and the fluorescence of NPs (*red*) detected in the nuclei of the same cells (excitation filter of 530–550 nm emission filter of 590 nm). (Color figure online)

RGD-Aptamer, once internalized in C6 cell, can be attributed to the aggregation-induced emission phenomenon [27]. ^{177}Lu-NP-conjugates may undergo an aggregation phenomenon that modifies their physical properties and enhances the fluorescence present in NPs colloidal systems. ^{177}Lu-NP-NLS-RGD-Aptamer showed larger mean intensity that the rest of the treatments (Fig. 7), which is correlated with a strong fluorescence phenomenon present inside the cells.

Conclusions

TEM, DLS and spectroscopy techniques demonstrated that NPs could be successfully conjugated to NLS-RGD and HS-pentyl-pegaptanib (aptamer) through interactions with the thiol groups of cysteine. ^{177}Lu-NP-NLS-RGD-Aptamer, with a radiochemical purity >98%, is highly stable in human serum and shows specific recognition for $\alpha(v)\beta(3)$ integrin and VEGF (in vitro inhibition of vascular-tube formation). The cancer-specific ^{177}Lu-Au-nanoradiopharmaceutical shows suitable properties as a specific antiangiogenic agent by targeting both the VEGF pathway and $\alpha(v)\beta(3)$ integrin. The results obtained in this study warrant further preclinical studies to determine the in vivo specificity and the radio-therapeutic and antiangogenic properties of the ^{177}Lu-NP-NLS-RGD-Aptamer radiopharmaceutical.

References

1. Yook S, Cai Z, Lu Y, Winnik MA, Pignol J, Reilly RM (2015) Radiation nanomedicine for EGFR-positive breast cancer: pani-tumumab-modified gold nanoparticles complexed to the β-particle-emitter, (177)Lu. Mol Pharm 12:3963–3972
2. Ferro-Flores G, Ocampo-García BE, Santos-Cuevas CL, De Maria Ramirez F, Azorin-Vega EP, Meléndez-Alafort L (2015) Theranostic radiopharmaceuticals based on gold nanoparticles labeled with ^{177}Lu and conjugated to peptides. Curr Radiopharm 8:150–159
3. Banerjee S, Pillai M, Knapp F (2015) Lutetium-177 therapeutic radiopharmaceuticals: linking chemistry, radiochemistry, and practical applications. Chem Rev 115:2934–2974
4. Lopes-Bastos BM, Jiang WG, Cai J (2016) Tumour-endothelial cell communications: important and indispensable mediators of tumour angiogenesis. Anticancer Res 36:1119–1126
5. Frezzetti D, Gallo M, Roma C, D'Alessio A, Maiello MR, Bevilacqua S, Normanno N, De Luca A (2016) Vascular endothelial growth factor regulates the secretion of different angiogenic factors in lung cancer cells. J Cell Physiol 231:1514–1521
6. Lin Z, Zhang Q, Luo W (2016) Angiogenesis inhibitors as therapeutic agents in cancer: challenges and future directions. Eur J Pharmacol 793:76–81
7. Hoffmann S, He S, Jin M, Ehren M, Wiedemann P, Ryan SJ, Hinton DR (2005) A selective cyclic integrin antagonist blocks the integrin receptors $\alpha_v\beta_3$ and $\alpha_v\beta_5$ and inhibits retinal pigment epithelium cell attachment, migration and invasion. BMC Ophthalmol 5:16
8. Ellert-Miklaszewska A, Poleszak K, Kaminska B (2017) Short peptides interfering with signaling pathways as new therapeutic tools for cancer treatment. Future Med Chem 9:199–221

9. Ocampo-García BE, Santos-Cuevas CL, De León-Rodríguez LM, García-Becerra R, Ordaz-Rosado D, Luna-Guitiérrez MA, Jiménez-Mancilla NP, Romero-Piña ME, Ferro-Flores G (2013) Design and biological evaluation of ^{99m}Tc-N$_2$S$_2$-Tat (49–57)-c(RGDyK): a hybrid radiopharmaceutical for tumors expressing α(v)β(3) integrins. Nucl Med Biol 40:481–487

10. Xiang D, Shigdar S, Qiao G, Wang T, Kouzani AZ, Zhou SF, Kong L, Li Y, Pu C, Duan W (2015) Nucleic acid aptamer-guided cancer therapeutics and diagnostics: the next generation of cancer medicine. Theranostics 5:23

11. Zhou G, Wilson G, Hebbard L, Duan W, Liddle C, George J, Qiao L (2016) Aptamers: a promising chemical antibody for cancer therapy. Oncotarget 7:13446

12. Davis GE, Senger DR (2005) Endothelial extracellular matrix, biosynthesis, remodeling, and functions during vascular morphogenesis and neovessel stabilization. Circ Res 97:1093–1107

13. Shallal HM, Minn I, Banerjee SR, Lisok A, Mease RC, Pomper MG (2014) Heterobivalent agents targeting PSMA and integrin-α$_v$β$_3$. Bioconjugate Chem 25:393–405

14. Zhang J, Niu G, Lang L, Li F, Fan X, Yan X, Yao S, Yan W, Huo L, Chen L (2017) Clinical translation of a dual integrin α$_v$β$_3$–and gastrin-releasing peptide receptor–targeting PET radiotracer, ^{68}Ga-BBN-RGD. J Nucl Med 58:228–234

15. Eder M, Schäfer M, Bauder-Wüst U, Haberkorn U, Eisenhut M, Kopka K (2014) Preclinical evaluation of a bispecific low-molecular heterodimer targeting both PSMA and GRPR for improved PET imaging and therapy of prostate cancer. Prostate 74:659–668

16. Morales-Avila E, Ferro-Flores G, Ocampo-García BE, De León-Rodríguez LM, Santos-Cuevas CL, García-Becerra R, Medina LA, Gómez-Oliván L (2011) Multimeric system of ^{99m}Tc-labeled gold nanoparticles conjugated to c[RGDfK(C)] for molecular imaging of tumor α(v)β(3) expression. Bioconjugate Chem 22:913–922

17. Luna-Gutiérrez M, Ferro-Flores G, Ocampo-García BE, Santos-Cuevas CL, Jiménez-Mancilla N, León-Rodríguez D, Azorín-Vega E, Isaac-Olivé K (2013) A therapeutic system of 177Lu-labeled gold nanoparticles-RGD internalized in breast cancer cells. J Mex Chem Soc 57:212–219

18. Aranda E, Owen GI (2009) A semi-quantitative assay to screen for angiogenic compounds and compounds with angiogenic potential using the EA.hy926 endothelial cell line. Biol Res 42:377–389

19. Vilchis-Juárez A, Ferro-Flores G, Santos-Cuevas C, Morales-Avila E, Ocampo-García BE, Díaz-Nieto L, Luna-Gutiérrez M, Jiménez-Mancilla N, Pedraza-López M, Gómez-Oliván L (2014) Molecular targeting radiotherapy with cyclo-RGDFK (C) peptides conjugated to 177Lu-labeled gold nanoparticles in tumor-bearing mice. J Biomed Nanotechnol 10:393–404

20. Socrates G (2004) Infrared and Raman characteristic group frequencies: tables and charts. Wiley, New Jersey

21. Jiménez-Mancilla N, Ferro-Flores G, Santos-Cuevas C, Ocampo-García B, Luna-Gutiérrez M, Azorín-Vega E, Isaac-Olivé K, Camacho-López M, Torres-García E (2013) Multifunctional targeted therapy system based on ^{99m}Tc/^{177}Lu-labeled gold nanoparticles-Tat (49–57)-Lys^3-bombesin internalized in nuclei of prostate cancer cells. J Labelled Compd Radiopharm 56:663–671

22. Pan Y, Ding H, Qin L, Zhao X, Cai J, Du B (2013) Gold nanoparticles induce nanostructural reorganization of VEGFR2 to repress angiogenesis. J Biomed Nanotechnol 9:1746–1756

23. Kang B, Mackey MA, El-Sayed MA (2010) Nuclear targeting of gold nanoparticles in cancer cells induces DNA damage, causing cytokinesis arrest and apoptosis. J Am Chem Soc 132:1517–1519

24. Dykman LA, Khlebtsov NG (2013) Uptake of engineered gold nanoparticles into mammalian cells. Chem Rev 114:1258–1288

25. Zhang J, Liu B, Liu H, Zhang X, Tan W (2013) Aptamer-conjugated gold nanoparticles for bioanalysis. Nanomedicine 8:983–993

26. Yeom JH, Joo M, Lee B, Kim KP, Ha NC, Park Y, Bae J, Lee K (2017) Intracellular delivery of recombinant proteins via gold nanoparticle-DNA aptamer composites is independent of the protein physicochemical properties and cell type. J Ind Eng Chem 45:5–10

27. Goswami N, Yao Q, Luo Z, Li J, Chen T, Xie J (2016) Luminescent metal nanoclusters with aggregation-induced emission. J Phys Chem Lett 7:962–975